Tuning the Au-Free InSb Nanocrystal Morphologies Grown by Patterned Metal–Organic Chemical Vapor Deposition

Andrew Lin, Joshua N. Shapiro, Holger Eisele,* and Diana L. Huffaker**

A thorough study of direct InSb nanocrystal formations on patterned InAs (111)B substrates is provided. These nanostructures are created without the use of Au catalysts or initial InAs segments. Under the growth conditions generally used for selective-area, catalyst-free epitaxy, a wide range of InSb nanocrystal morphologies are observed. This is because the low-energy InSb surfaces, studied by first-principles calculations, are the {111} facets as opposed to the {110} facets. By controlling the V/III ratio during growth, different InSb nanostructures can be achieved. Using low V/III growth conditions, In droplets start to form and InSb nucleation takes place at the droplet–semiconductor interface only, resulting in vertical, self-catalyzed InSb nanopillars.

1. Introduction

Extensive research efforts have been devoted to the studies and developments of III-V semiconductor nanowires (NWs) and nanopillars (NPs) because of their unique physical properties and ability to form high quality, highly lattice-mismatched axial and radial heterostructures. To date, functional optoelectronic and electronic devices based on these NP heterostructures have been successfully demonstrated, including tunnel diodes,[1,2] vertical surround-gate transistors,[3,4] light-emitting diodes,[5,6] lasers,[7,8] photodetectors,[9] and photovoltaics.[10,11] In the past, InSb has attracted special attention for its potential as high-speed electronics[12] and mid-IR emitters and detectors[13,14] because it has the highest bulk electron and hole mobilities (μ_e of 77 000 cm^2/Vs and μ_h of 850 cm^2/Vs) and the smallest band-gap (0.17 eV) in all III–V semiconductors.[15] Furthermore, having a large Bohr exiton radius (>60 nm) and a high electron magnetic moment ($g^* \sim 51$),[16,17] InSb nanostructures are viewed as an ideal vehicle to experimentally study quantum physical phenomena and spin-orbit systems.[18–20] Despite these attractive properties, advanced development in InSb-based technology has been difficult because of a lack of semi-insulating, lattice-matched substrates, and convoluted epitaxial constraints. Recent progress in nano-heteroepitaxy, however, has enabled high-quality III-V NPs to form on highly lattice-mismatched substrates.[3,21] This advancement opens the door for heterogeneous integration of high-performance InSb NP devices on cheaper and more readily available platforms.

Exploration of InSb in the NP community is a growing research interest, with the first reports appearing in 2005. InSb NPs have been grown using Au-assisted chemical beam epitaxy,[22,23] Au-catalyzed metal-organic chemical vapor deposition (MOCVD),[24–26] thermal CVD,[27] electrodeposition in porous templates,[28] and self-nucleation.[29] Almost all recently published methods are based on epitaxial techniques that generally use Au catalysts and an initial formation of InAs NP segments to assist the InSb NP formation. However, there has been evidence of Au atom contamination in the NPs using Au-catalyzed growth[30]; Au is known to create recombination centers in III-V semiconductors. This can significantly reduce the minority carrier lifetime and increase scattering, therefore hampering the device performance. Moreover, the necessity of using short InAs segments to assist InSb NP formation can further complicate practical device fabrication because of the large band-offset and type-III, broken-gap band alignment between InAs and InSb.[31]

In this work, we provide a thorough study of direct InSb nanostructure formation on patterned InAs (111)B substrates, by MOCVD, without the use of Au catalysts and short InAs segments. We investigate various growth conditions that result in different types of InSb nanostructures, including the conditions required to achieve vertical NP growth. Our observations are then explained by first-principles calculations using density-function theory (DFT). This paper provides a basic ground work for potential optoelectronic and electronic devices based on Au-free InSb NPs.

2. Methods

InSb nanostructures are grown on patterned InAs (111)B substrates with a low-pressure (60 torr) vertical Emcore MOCVD reactor, using trimethylindium (TMIn) and trimethylantimony (TMSb) as precursors. The InAs substrates are patterned with

A. Lin, J. N. Shapiro, D. L. Huffaker
Department of Electrical Engineering
University of California at Los Angeles
Los Angeles, CA 90095, USA
E-mail: andrewlin@ucla.edu; huffaker@ee.ucla.edu
H. Eisele
Institut für Festkörperphysik
Technische Universität Berlin
Hardenbergstr.36
10623, Berlin, Germany
D. L. Huffaker
California Nano-Systems Institute
University of California
Los Angeles, CA 90095, USA

DOI: 10.1002/adfm.201303390

a SiO_2 mask (20-nm thick) using e-beam lithography and reactive ion etching, with a nanohole opening of 70 nm and a pitch of 500 nm. The patterned growth allows for a precise control over the position of nanostructure formation, leading to simpler device fabrication and enabling interesting new device functionalities such as bottom-up photonic crystals and plasmonic gratings using these patterned nanostrctures.[7,9] The growth temperature in this study is limited by the low melting temperature of InSb (530 °C) at one side and the cracking temperature of TMSb precursor (>450 °C) at the other one. We have explored different growth temperatures ranging from 460 to 500 °C with no discernible impact on the growths. All the InSb growths presented in the study are carried out at a substrate temperature of 470 °C by flowing TMIn and TMSb under varying V/III ratios. The V/III ratio is controlled by fixing the TMIn flow while changing the TMSb flow. We note that the supplied Sb adatoms tend to form Sb clusters at the growth surface and these clusters need to be dissociated before being incorporated into InSb growth. Because this dissociation ratio is not perfect, the effective reacting V/III ratio is different from the supplied V/III ratio. In the interest of simplicity, the V/III ratio addressed in this paper refers to the supplied V/III ratio. After growth, the samples are cooled down under Sb overpressure to prevent InSb desorption. The resulting structures are studied by scanning electron microscopy (SEM) using an FEI Nova SEM/FIB system to determine the InSb nanocrystal formation and morphology. Further structural properties and chemical analyses are examined by transmission electron microscopy (TEM) and energy dispersive X-ray spectroscopy (EDX) using a FEI Titan 300 kV S/TEM system. Cross-sectional TEM samples are prepared by the FIB.

To theorize the observed InSb nanocrystal formations, first-principles computations using density-functional theory (DFT) are carried out to determine the surface energies of different InSb surfaces. These calculations are performed with the software package FHI-AIMS,[32] which utilizes numeric atom centered orbitals for its basis set and includes a relativistic correction for heavy atoms (Z > 30). The Perdew-Burke-Ernzerhof (PBE) parameterization of the generalized gradient approximation is used for the exchange-correlation functional.[33] A detailed description on the DFT simulation can be found in the Supporting Information.

3. Results and Discussion

The InSb growths by MOCVD are extremely sensitive to the local environments. A series of growths using V/III ratios ranging from 0.3 to 2 with a growth time of 7 minutes is depicted in the tilted SEM images in **Figure 1**. Evidently, the resulting InSb morphologies can be controlled by tuning the V/III ratios. Under a V/III of 2 (Figure 1d), hexagonal pancake-like InSb structures with a flat (111)B top surface and {110} sidewalls are observed with minimal vertical growth and an average height and diameter of 80 nm and 400 nm,

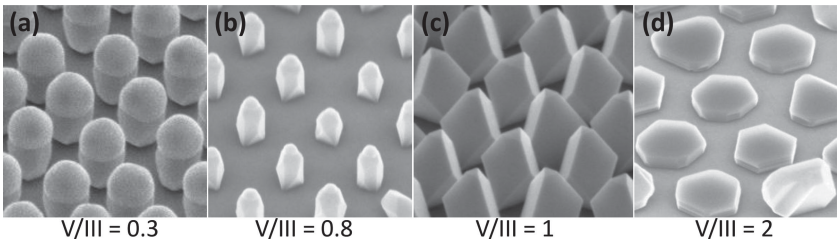

Figure 1. Tilted SEM images (52°) of InSb growths at 470 °C using V/III ratios ranging from 0.3 to 2 and a growth time of 7 min.

respectively. By lowering the V/III ratio, more vertical InSb structures start to form. Using a V/III of 1 (Figure 1c) results in truncated InSb octahedrons with small, triangular (111)B top surfaces and inclined side facets. The average height of these truncated octahedrons is 300 nm. Lowering the V/III to 0.8 leads to yet another different structure resembling NP-like InSb formations (h = 250 nm, d = 140 nm) with In droplets on the top (Figure 1b). The In droplets become more prominent using an even lower V/III of 0.3 (more In-rich), hence forming larger droplets and, consequently, InSb NPs with larger diameters (h = 410 nm, d = 290 nm), as shown in Figure 1a. Typically, in other III-V semiconductor systems, catalyst-free, selective-area NPs take the shape of a hexagonal pillar with (111)B top surfaces and {110} sidewalls because {110} surfaces have the lowest surface energy. In the case of InSb, however, surfaces with the lowest energy appear to be different. This discrepancy posts difficulty for selective-area, catalyst-free InSb NP formation. Using low V/III ratios, or In-rich conditions, In droplets form and the vertical, self-catalyzed NP is initiated between the substrate and droplets. Without the In droplets, In and Sb adatoms diffuse and relax based on the surface energetics to form the InSb equilibrium surfaces that result in non-NP growth.

Cross-sectional TEM is carried out on the InSb truncated octahedron formations shown in Figure 1c to identify the preferred InSb surfaces and study the crystal structure. **Figure 2**a shows a TEM image of a single InSb truncated octahedron with side facets at different angles. The top flat facet is identified as a (111)B surface, being parallel to the InAs (111)B growth substrate. A close-up TEM image (Figure 2b) shows that the truncated octahedron is of single crystal zinc-blende (ZB) structure without any stacking fault or wurtzite (WZ) region. The latter is commonly observed in other NP material systems such as GaAs[34] and InAs.[35] This is likely because of the lower growth temperature (470 °C) and larger energy difference between zinc-blende (ZB) and wurtzite (WZ) InSb. Indeed, the fast Fourier transform (FFT) image of this close-up region (inset of Figure 2b) shows a purely ZB crystal structure. The normal angle between the top (111)B and the inclined side surfaces is measured to be 70.5°, indicating the {111}A inclined surfaces. The TEM analysis concludes that this InSb nanostructure is dominated by the {111} surfaces, an indication that these are the preferred low-energy surfaces in the InSb materials system.

Surface energies for the three observed crystal facets are calculated using DFT to understand how to control the nanocrystal morphology with V/III ratios. **Figure 3** shows the surface energy, γ, versus the calculated Sb chemical potential, μ_{Sb}, for the lowest energy reconstructions of the (111)A and (111)B, and

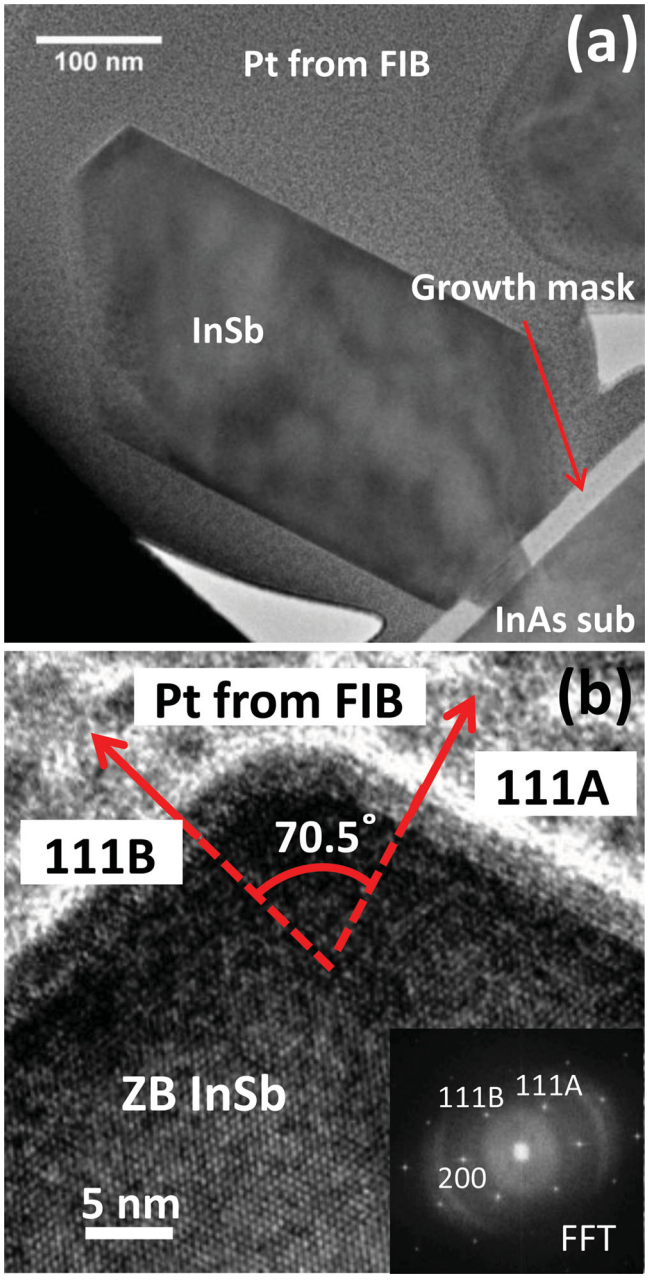

Figure 2. (a) Cross-sectional TEM image of the InSb truncated octahedron grown at a V/III = 1, showing the different surfaces. (b) Close-up of the TEM image showing purely ZB InSb and the (111)B top and (111)A side surfaces with an inset of the FFT to identify the crystal structure and different surfaces.

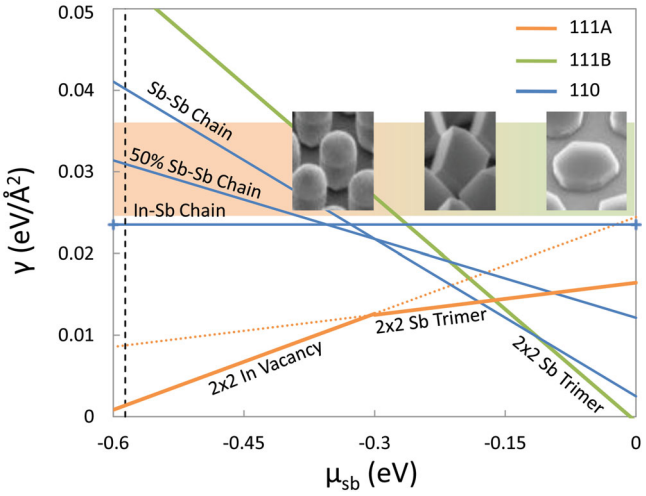

Figure 3. A phase diagram of surface energy for the 111A (orange), 111B (green), and 110 (blue) surface vs. chemical potential of Sb. Important surface reconstructions for each surface are shown as solid lines where they are dominant and as dashed lines otherwise. SEM images of nanocrystals are approximately positioned along the x-axis where the calculated surface energies can produce the observed shape.

for the 110 terminated with In-Sb chains, Sb-Sb chains, and an equal mix of the two chains (see supporting information). Top views of the atomic surfaces are shown in **Figure 4**. Also shown in Figure 3 are the cropped SEM images of InSb nanocrystals grown at different V/III ratios. Their position along the x-axis roughly corresponds to the surface energies required to reproduce the observed morphology, and the color of the shaded background corresponds to the dominant surface. Large values of μ_{Sb} represent Sb-rich conditions and high V/III ratios, and small values of μ_{Sb} represent In-rich conditions and low V/III ratios. The vertical dashed line at $\mu_{Sb} = -0.58$ is the calculated enthalpy of formation of InSb, which represents the lower bound of possible values for μ_{Sb}. Comparing the observed crystal structure with the calculated surface energies, it is possible to determine an empirical relationship between V/III ratio and the chemical potential, and ultimately learn the range of crystal morphologies for InSb.

The SEM images are correlated to ranges of μ_{Sb} on the phase diagram in Figure 3 by inspection. At the far right is a nanocrystal whose shape is dominated by a large (111)B surface and flanked by {110} surfaces. This shape is consistent with the right of the phase diagram when $\gamma_{111B} < \gamma_{110} < \gamma_{111A}$. The intermediate nanocrystal shape is dominated by (111)A surfaces with small (111)B surfaces in a truncated octahedron and with no evidence of (110) surfaces. Such a shape will be observed if $\gamma_{111A} < \gamma_{111B} < \gamma_{110}$, however this inequality cannot be satisfied unless the (110) surface is <100% terminated with Sb-Sb chains. For example, a small region from $-2.1 < \mu_{Sb} < -1.6$ can satisfy the inequality if the (110) surface is 50% terminated with Sb-Sb chains. At the left side of the figure, the {110} surfaces become visible and the (111)B surface area shrinks indicating $\gamma_{111A} < \gamma_{110} < \gamma_{111B}$. This situation occurs easily because of the steep rise in the (111)B surface energy as μ_{Sb} decreases.

These calculations verify that surface energy plays an important role in determining the shape of a nanocrystal grown by selective-area-epitaxy, but simultaneously indicate that there are other important physical effects driving the crystal growth. In particular, the apparent ability of the {110} surfaces to reconstruct in less energetically favorable configurations where the surface is only partially terminated with Sb reinforces the need to consider kinetic effects such as adatom diffusion and exchange with surface atoms. Nevertheless, this phase-diagram permits us to make some predictions and control over allowed and disallowed InSb nanocrystal morphologies. For instance,

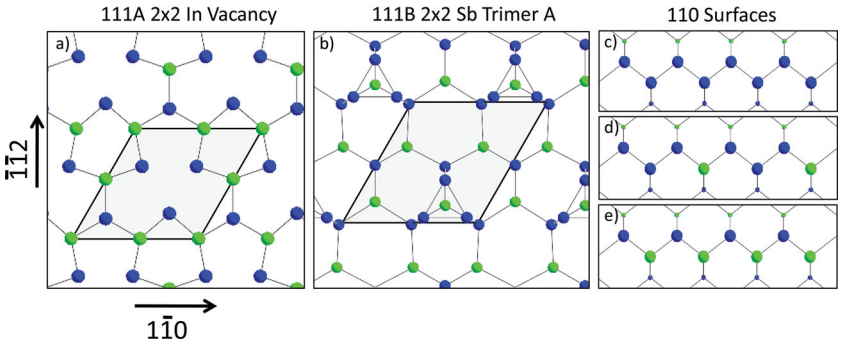

Figure 4. a) The 111A In Vacancy surface reconstruction. b) The 111B Sb Trimer surface reconstruction. c) The 110 Sb-Sb Chain. d) The 110 50% Sb-Sb Chain. e) The 110 In-Sb Chain. The unit cell is outlined and shaded for the 111A and 111B surfaces. In atoms are green, and Sb atoms are blue.

we predict it is very unlikely to observe an InSb pillar shape with large {110} surface area, a small (111)B surface, and no (111)A surfaces using only selective-area, catalyst-free epitaxy.

With the In droplets, vertical InSb growths can be achieved. On the other hand, if the droplets are not maintained throughout the growth, the preferred {111} facets will form, inhibiting vertical NP growth. Taking a closer look at the InSb NP growth with a V/III ratio of 0.8 from Figure 1b, one can see that there are In droplets with varying sizes. This is likely because the V/III ratio of 0.8 is near the transition from purely selective-area epitaxy to self-catalyzed conditions that form In droplets. **Figure 5** shows several top-view SEM images of these InSb NPs with different In droplet dimensions to show the progression of InSb NP formation with diminishing In droplets. The NP formation appears to follow closely with In droplet, leading to hexagonal NPs with {110} side facets (Figure 5a).

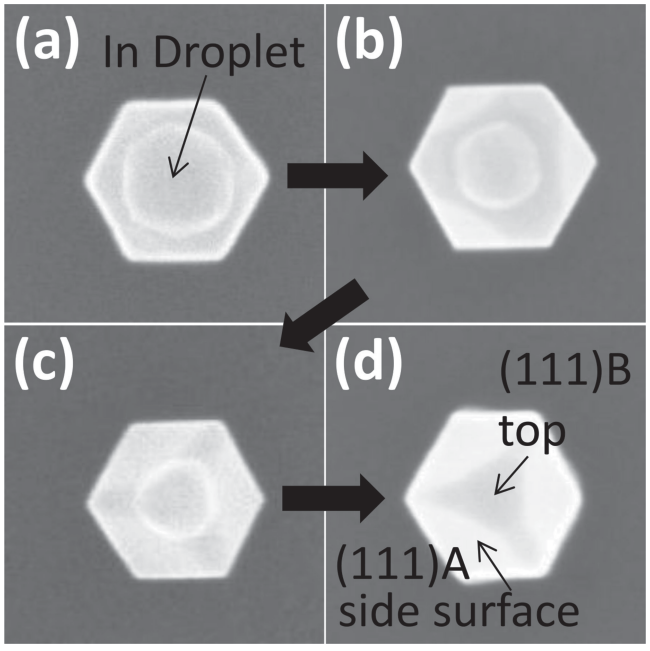

Figure 5. Top view SEM images of InSb NPs grown at 470 °C using a V/III ratio of 0.8 showing the progression of the inclined sidewall formation with disappearing In droplet.

When the In-rich condition is not maintained, the In droplet gets incorporated into InSb NP and the three inclined {111}A surfaces begin to form (Figure 5b). As the In droplet shrinks, different InSb facets start to form (Figure 5c) and eventually the entire droplet is absorbed by the InSb NP that result in three inclined {111}A side facets and a small top (111)B surface (Figure 5d). From these observations, we can conclude that In droplets are necessary to maintain vertical InSb NP growth. Under constant In-rich conditions, however, the In droplets also grow in size as growth time increases and larger droplets lead to NPs with much larger dimensions. A 15-minute InSb NP growth using a constant V/III ratio of 0.7 result in NPs with 500 nm diameter (SEM not shown). To accomplish taller NPs with smaller diameters, another approach must be developed.

In order to achieve NPs with higher aspect ratio, we implement a two-step growth technique. The growth starts with self-catalyzed growth under a low V/III ratio of 0.7 for 7 min. We choose this initial V/III ratio because any lower ratios would result in larger droplets rather quickly. Then, the V/III is raised to 0.9 for another 7 min in order to maintain the droplet size to achieve taller NPs, while keeping the NP diameter reasonably small. The SEM of the resulting growth is depicted in **Figure 6**a, showing InSb NPs with an average height and diameter of 780 nm and 250 nm, respectively. The TEM image (Figure 6b) shows a purely ZB InSb NP with an In droplet on the top. The twin-free, self-catalyzed InSb NPs have several advantages to avoid potential problems posted by stacking faults. The energy difference between ZB and WZ structures can lead to increased carrier scattering and reduced transport properties. The twinning can also further complicate band structure design in homo- or heterostructures. The InSb NP has flat {110} sidewalls with small (111)A and (111)B inclined surfaces near the base and the NP-droplet interface. An EDX scan along the length of the NP is used to analyze the chemical composition of the NP. The scan indicates an In droplet formation on the tip of NP and an equal amount of In and Sb atoms in the NP. We note that the scan shows that there are Sb atoms in the droplet, which is likely an artifact from the scan because the In and Sb energies have some overlap in the EDX spectrum. Using such a two-step growth mode, we have realized vertical, pure ZB, self-catalyzed InSb NPs on patterned InAs (111)B substrates without the use of any Au catalysts or initial InAs NP growth. We believe by further fine-tuning this approach, such as different combinations of V/III ratios in the two-step growth or multiple two-step cycles in one growth, taller and smaller InSb NPs can be achieved.

4. Conclusion

We have investigated the growth conditions for InSb NPs directly on patterned InAs (111)B substrates. From the observed growths and DFT computations on different InSb surfaces, we show how the InSb nanocrystal morphologies can be controlled

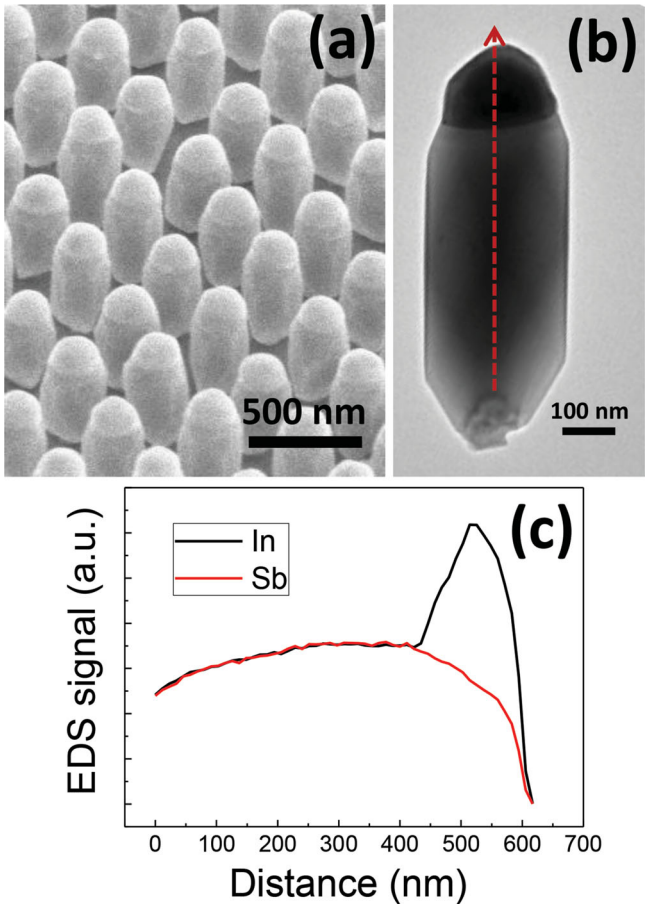

Figure 6. (a) A tilted SEM image showing InSb NPs resulted from the two-step growth. (b) A TEM image of a purely ZB InSb NP. (c) EDX of an InSb NP showing the In-rich droplet.

by tuning the V/III ratios. At higher V/III ratios (>1), pancake-like and truncated octahedron InSb structures form because the energetically favorable surfaces are the {111} facets as opposed to the {110} facets. Therefore, vertical InSb NP cannot be achieved via the selective-area, catalyst-free method. Using lower V/III ratios, In droplet forms in the mask opening that results in vertical InSb self-catalyzed NP growth. Constant In-rich conditions, however, lead to increasing In droplet sizes that forms NPs with large dimensions. A two-step growth mode is then used to attain InSb NPs with higher aspect ratio and smaller dimensions.

Supporting Information

Supporting Information is available from the Wiley Online Library or from the author.

Acknowledgements

The authors thank the financial support by NSF through (ECCS-0824273), (DMR-1309137), and (DMR-1007051), and by DoD through (NSSEFF N00244-09-1-0091).

Received: October 1, 2013
Published online: April 6, 2014

[1] J. Wallentin, J. M. Persson, J. B. Wagner, L. Samuelson, K. Deppert, M. T. Borgström, *Nano Lett.* **2010**, *10*, 974.
[2] C. D. Bessire, M. T. Björk, H. Schmid, A. Schenk, K. B. Reuter, H. Riel, *Nano Lett.* **2011**, *11*, 4195.
[3] K. Tomioka, M. Yoshimura, T. Fukui, *Nature* **2012**, *488*, 189.
[4] M. Egard, S. Johansson, A. C. Johansson, K. M. Persson, A. W. Dey, B. M. Borg, C. Thelander, L. E. Wernersson, E. Lind, *Nano Lett.* **2010**, *10*, 809.
[5] O. Hayden, A. B. Greytak, D. C. Bell, *Adv. Mater.* **2005**, *17*, 701.
[6] K. Tomioka, J. Motohisa, S. Hara, K. Hiruma, T. Fukui, *Nano Lett.* **2010**, *10*, 1639.
[7] A. C. Scofield, S.-H. Kim, J. N. Shapiro, A. Lin, B. Liang, A. Scherer, D. L. Huffaker, *Nano Lett.* **2011**, *11*, 5387.
[8] F. Qian, Y. Li, S. Gradecak, H.-G. Park, Y. Dong, Y. Ding, Z. L. Wang, C. M. Lieber, *Nat. Mater.* **2008**, *7*, 701.
[9] P. Senanayake, C.-H. Hung, J. Shapiro, A. Lin, B. Liang, B. S. Williams, D. L. Huffaker, *Nano Lett.* **2011**, *11*, 5279.
[10] J. Tang, Z. Huo, S. Brittman, H. Gao, P. Yang, *Nat. Nanotechnol.* **2011**, *6*, 568.
[11] G. Mariani, P.-S. Wong, A. M. Katzenmeyer, F. Léonard, J. Shapiro, D. L. Huffaker, *Nano Lett.* **2011**, *11*, 2490.
[12] B. R. Bennett, R. Magno, J. B. Boos, W. Kruppa, M. G. Ancona, *Solid-State Electron.* **2005**, *49*, 1875.
[13] E. Michel, J. Xu, J. D. Kim, I. Ferguson, M. Razeghi, *Photonics Technol. Lett. IEEE* **1996**, *8*, 673.
[14] L. P. Chen, J. J. Lou, T. H. Liu, Y. M. Pang, S. J. Yang, *Solid-State Electronics* **1992**, *35*, 1081.
[15] I. Vurgaftman, J. R. Meyer, L. R. Ram-Mohan, *J. Appl. Phys.* **2001**, *89*, 5815.
[16] R. A. Isaacson, *Phys. Rev.* **1968**, *169*, 312.
[17] H. A. Nilsson, P. Caroff, C. Thelander, M. Larsson, J. B. Wagner, L.-E. Wernersson, L. Samuelson, H. Q. Xu, *Nano Lett.* **2009**, *9*, 3151.
[18] V. Mourik, K. Zuo, S. M. Frolov, S. R. Plissard, E. P. A. M. Bakkers, L. P. Kouwenhoven, *Science* **2012**, *336*, 1003.
[19] L. P. Rokhinson, X. Liu, J. K. Furdyna, *Nat. Phys.* **2012**, *8*, 795.
[20] J. Liu, A. C. Potter, K. T. Law, P. A. Lee, *Phys. Rev. Lett.* **2012**, *109*, 267002.
[21] X.-Y. Bao, C. Soci, D. Susac, J. Bratvold, D. P. R. Aplin, W. Wei, C.-Y. Chen, S. A. Dayeh, K. L. Kavanagh, D. Wang, *Nano Lett.* **2008**, *8*, 3755.
[22] E. Daniele, R. Francesca, L. Ang, R. Stefano, G. Vincenzo, S. Giancarlo, B. Fabio, S. Lucia, *Nanotechnology* **2009**, *20*, 505605.
[23] A. T. Vogel, J. de Boor, J. V. Wittemann, S. L. Mensah, P. Werner, V. Schmidt, *Crystal Growth Design* **2011**, *11*, 1896.
[24] P. Caroff, J. B. Wagner, K. A. Dick, H. A. Nilsson, M. Jeppsson, K. Deppert, L. Samuelson, L. R. Wallenberg, L.-E. Wernersson, *Small* **2008**, *4*, 878.
[25] S. R. Plissard, D. R. Slapak, M. A. Verheijen, M. Hocevar, G. W. G. Immink, I. van Weperen, S. Nadj-Perge, S. M. Frolov, L. P. Kouwenhoven, E. P. A. M. Bakkers, *Nano Lett.* **2012**, *12*, 1794.
[26] X. Yang, G. Wang, P. Slattery, J. Z. Zhang, Y. Li, *Crystal Growth Design* **2010**, *10*, 2479.
[27] H. D. Park, S. M. Prokes, M. E. Twigg, Y. Ding, Z. L. Wang, *J. Crystal Growth* **2007**, *304*, 399.
[28] Y. Yang, L. Li, X. Huang, G. Li, L. Zhang, *J. Mater. Sci.* **2007**, *42*, 2753.
[29] C. Pendyala, S. Vaddiraju, J. H. Kim, J. Jacinski, Z. Chen, M. K. Sunkara, *Semiconductor Sci. Technol.* **2010**, *25*, 024014.
[30] J. E. Allen, E. R. Hemesath, D. E. Perea, J. L. Lensch-Falk, Z. Y. Li, F. Yin, M. H. Gass, P. Wang, A. L. Bleloch, R. E. Palmer, L. J. Lauhon, *Nat. Nanotechnol.* **2008**, *3*, 168.
[31] S.-H. Wei, A. Zunger, *Phys. Rev. B* **1995**, *52*, 12039.

[32] V. Blum, R. Gehrke, F. Hanke, P. Havu, V. Havu, X. Ren, K. Reuter, M. Scheffler, *Computer Phys. Commun.* **2009**, *180*, 2175.
[33] J. P. Perdew, K. Burke, M. Ernzerhof, *Phys. Rev. Lett.* **1996**, *77*, 3865.
[34] A. Lin, J. N. Shapiro, P. N. Senanayake, A. C. Scofield, P.-S. Wong, B. Liang, D. L. Huffaker, *Nanotechnology* **2012**, *23*, 105701.
[35] A. Lin, J. N. Shapiro, A. C. Scofield, B. L. Liang, D. L. Huffaker, *Appl. Phys. Lett.* **2013**, *102*, 053115.